3 AHN, D., PARK, J-S., KIM, C-S., KIM, J., QIAN, Y., and ITOH, T.: 'A design of the low-pass filter using the novel microstrip defected ground structure', *IEEE Trans. Microw. Theory Tech.*, 2001, **49**, pp. 86–91
4 D'ORAZIO, A., DE SARIO, M., GADALETA, V., PETRUZZELLI, V., and PRUDENZANO, F.: 'A meander microstrip photonic bandgap filter using a Kaiser tapering window', *Electron. Lett.*, 2001, **37**, pp. 1165–1167

Equivalent circuit modelling of spiral defected ground structure for microstrip line

Chul-Soo Kim, Jong-Sik Lim, Sangwook Nam, Kwang-Yong Kang and Dal Ahn

An equivalent circuit for the microstrip line with a spiral defected ground structure (DGS), which is etched on the metallic ground plane, and a parameter extraction method, are presented. The proposed spiral DGS provides steep rejection characteristics with only one spiral-shaped defect. Experimental results show excellent agreement with simulated results of the equivalent circuit and the validity of equivalent circuit modelling for the spiral DGS.

Introduction: Microstrip transmission lines incorporating a defected ground structure (DGS) with periodic or non-periodic array exhibit bandgap and slow-wave characteristics such as periodic PBG structures [1, 2]. The band rejection and slow-wave characteristics of DGS are available to a power amplifier, divider, filters, etc. [3, 4]. In this Letter, we propose a spiral DGS and its equivalent circuit. This structure provides a greatly increasing effective inductance and capacitance to microstrip line. The equivalent circuit parameters for the spiral DGS consist of an inductor and a shorted stub. They are extracted on the basis of a circuit theory and field analysis method. The validity of the modelling method for the proposed spiral DGS is verified by experiments.

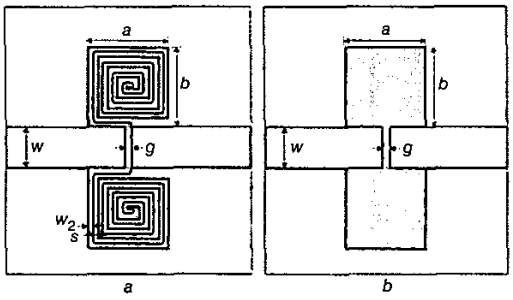

Fig. 1 *Schematic diagrams of defected ground structure*
a Spiral DGS
b Dumbbell DGS
$a = b = 5$ mm, $w2 = g = 0.4$ mm, $w = 2.4$ mm, and $s = 0.2$ mm

Characteristics and equivalent circuit: Fig. 1 shows schematic diagrams of a spiral and a dumbbell DGS with the same occupied surface area. The greyed section in Fig. 1 shows the etched spiral shape, which is located on the metallic ground plane. The substrate for simulation and measurement is the RT/Duroid 5880 with thickness of 31 mil and a dielectric constant (ε_r) of 2.2. The line width is chosen for the characteristic impedance of 50 Ω for a typical microstrip line.

Fig. 2 shows the simulation results of the dumbbell and spiral DGS, respectively. As shown in the Figure, the attenuation pole of the spiral DGS shifts much lower than that of the dumbbell DGS in the same occupied surface area. Therefore, the spiral DGS can provide the size reduction of microstrip structure and steep rejection characteristics more efficiently than the dumbbell DGS. The equivalent circuit of the spiral DGS shown in Fig. 3*a* consists of an inductor and a shorted stub to represent a periodic frequency response. Here, Z_s is the characteristic impedance of the shorted stub and L_s indicates the inductance of cross-coupling between etched defect lines in the ground plane. Fig. 3*b* shows the Butterworth-type one pole lowpass filter. Equations (1) and (2) denote the susceptance of Figs. 3*a* and *b*, respectively:

$$B_s = -\left(Y_s \cot\theta + \frac{1}{\omega L_s}\right) \tag{1}$$

$$B_B = \frac{-1}{\omega L_B} \tag{2}$$

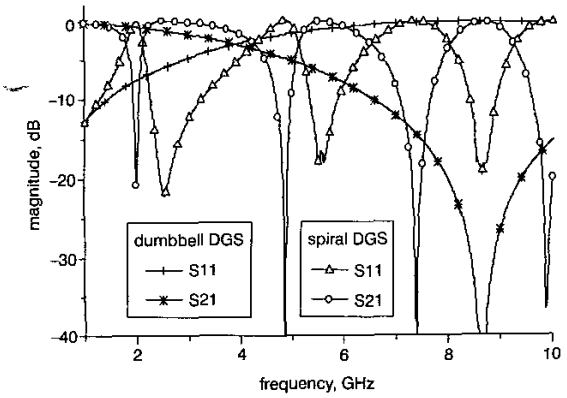

Fig. 2 *EM simulation results of proposed DGS*

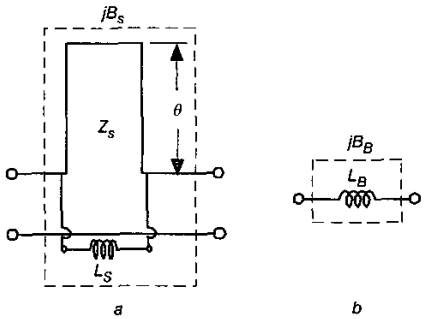

Fig. 3 *Equivalent circuit*
a Spiral DGS
b Butterworth-type one pole lowpass filter

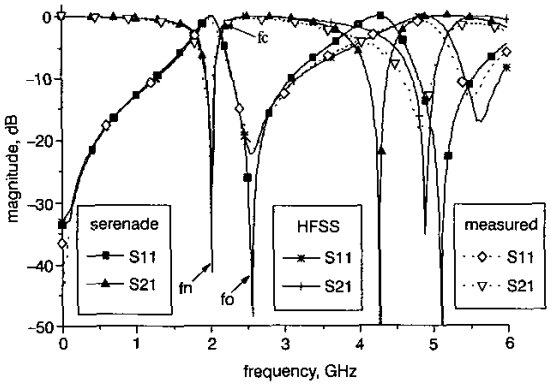

Fig. 4 *Simulated and measured results of spiral DGS*

The equivalent circuit parameters for the spiral DGS can be extracted from the simple circuit theory and EM simulation (HFSS) result shown in Fig. 4. Here, fn, fo, and fc indicate transmission zero, pole, and 3 dB cutoff frequency for the frequency response of the spiral DGS, respectively. From the resonance condition at 2.0 GHz (fn) and 2.55 GHz (fo), the susceptance and reactance of the equivalent circuit for the spiral DGS should be equal to zero, respectively. At 3 dB cutoff frequency (fc), (1) should be equal to (2). Using the above conditions, L_s and Z_s of the equivalent circuit are estimated to be 4.5 nH and 69.7 Ω, respectively. The electrical length (θ) of the shorted stub is 180° at 2.55 GHz (fo). Fig. 4 shows the comparison by simulation and

measurement for the spiral DGS. The experimental results show an excellent agreement with the simulated results of the equivalent circuit and the validity of equivalent circuit modelling.

Conclusions: We have presented a microstrip line with a spiral DGS and its equivalent circuit. The spiral DGS can provide the narrow stopband at lower frequency and steep rejection characteristics. Parameters of the equivalent circuit are extracted from the resonance condition and the relation with the Butterworth-type one pole lowpass filter. The experimental results show excellent agreement with the simulation results of the equivalent circuit and the validity of the modelling method for the spiral DGS. We expect that the proposed spiral DGS and circuit modelling can be applied to various microwave components.

4 February 2002
Electronics Letters Online No: 20020742
DOI: 10.1049/el:20020742

Chul-Soo Kim and Kwang-Yong Kang (*Telecommunication Basic Research Laboratory, ETRI, Yusong-Gu, Taejon, 305-600, Korea*)

Jong-Sik Lim and Sangwook Nam (*School of Electrical Engineering and Computer Science, Seoul National University, Seoul, 151-742, Korea*)

Dal Ahn (*Division of Information Technology Engineering, Soonchunhyang University, Asan, Chungnam, 336-745, Korea*)

References

1 RADISIC, V., QIAN, Y., COCCIOLI, R., and ITOH, T.: 'Novel 2D photonic bandgap structure for microstrip lines', *IEEE Microw. Guid. Wave Lett.*, 1998, **8**, pp. 69–72
2 QIAN, Y., YANG, F.R., and ITOH, T.: 'Characteristics of microstrip lines on a uniplanar compact PBG ground plane'. APMC, Dig., Yokohama, Japan, December 1998, pp. 589–592
3 LIM, J.S., KIM, H.S., PARK, J.S., AHN, D., and NAM, S.: 'A power amplifier with efficiency improved using defected ground structure', *IEEE Microw. Wirel. Compon. Lett.*, 2001, **11**, pp. 170–172
4 AHN, D., PARK, J.S., KIM, C.S., KIM, J., QIAN, Y., and ITOH, T.: 'A design of the low-pass filter using the novel microstrip defected ground structure', *IEEE Trans. Microw. Theory Tech.*, 2001, **49**, pp. 86–93

Miniature multilayer patch resonator

M. Simeoni, S. Verdeyme and C. Person

A novel miniature multilayer patch resonator is described. A non-radiative mode, induced by a centre via hole, leads to a miniaturised structure while maintaining a convenient Q-factor. The resonator is suitable for miniature band-pass filter design in multilayer self-shielded ceramic modules. Experimental results are presented and discussed.

Introduction: Recently, [1] the authors have presented a compact microstrip patch resonator with a via-hole connecting the ground plane: the rectangular wired-patch resonator. Its performances have been carefully investigated via full-wave electromagnetic simulations. Later [2] further work has confirmed the interesting features of this structure. The effect of adding the via-hole to a classic rectangular microstrip patch resonator is, as in the case of microstrip patch antennas [3], the appearance of a novel resonance named 'parallel resonance'. The parallel resonance is located at a low frequency compared to the classic cavity resonance of the patch. This new resonance enables an important reduction of the patch area for a given resonant frequency, in comparison with well-known hair-pin or circular loop resonators.

The structure presented in this Letter is a multilayer evolution of the rectangular wired-patch resonator; a further reduction of the patch surface is obtained. The new structure can exploit the possibilities offered by new technologies such as low temperature co-fired ceramics (LTCC) that enable the realisation of completely shielded multilayer ceramic structures with several metallised layers connected by mean of metal filled via-holes.

Working principle: In [1], the authors proposed a simple model of the rectangular wired-patch resonator. Two particular electrical behaviours can be observed at the parallel mode resonant frequency:

- the electric field is mainly located at the patch edges
- the magnetic field is mainly located around the via-hole

Then, an equivalent lumped network consisting of a parallel LC resonant circuit was proposed to model the structure. The self-inductive effect is associated with the displacement current flowing through the via-hole while the capacitive effect is associated with the electric energy stored at the patch periphery.

The frequency evolution observed when varying the different parameters of the structure confirms this rough physical interpretation.

The resonant frequency is virtually constant when changing the substrate thickness (h). This can be explained by the fact that increasing h, i.e. the length of the via-hole, results in a linear expansion of the value of L (the self inductance associated with the via-hole) while the value of C (the capacitance associated with the patch) linearly decreases. The product LC (hence the value of the resonant frequency) is therefore constant with h.

A slight decrease in the resonant frequency is observed when considering a thicker substrate for this rectangular wired-patch resonator; this can be explained by the increased weight of end effects.

The new idea is to separate the inductive and capacitive effects. Thus, the value of C may be modified without affecting the value of L, and therefore controlling the resonant frequency using various independent tuning parameters.

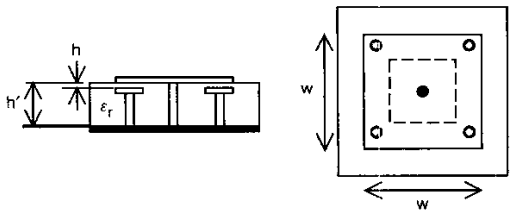

Fig. 1 *Side and top view of resonator*

Fig. 1 presents the proposed solution. The ground plane potential is raised, by means of four metallic via-holes, with a metallic ring located below the patch. This modification strongly increases the value of C and thus, lowers the parallel mode resonant frequency. It should be noted that the length of the central via-hole is not affected by the structure modification and the value of L is consequently virtually unchanged.

As a first approximation, the LC model can be maintained for the new structure since the four via-holes can be seen as a static connection without any associated self or mutual inductive effect. In fact they are four weak inductances connected in parallel by the metallic ring (that can be considered as an electric node since its length is a small portion of the resonant wavelength), and so the overall inductive effect can be neglected.

Fig. 2 shows the electric and magnetic field spatial distribution at the resonant frequency in a vertical and horizontal plane section. As can be seen, the electric field is well concentrated between the patch and metallic ring. The magnetic field is still mainly located around the central via-hole. Since the nature of the resonance is maintained, we will use in the following the same mode nomenclature.

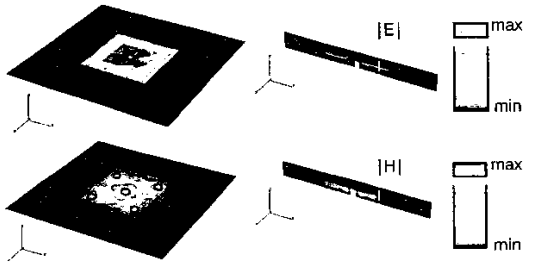

Fig. 2 *Field distribution at resonance frequency in horizontal and vertical sections*

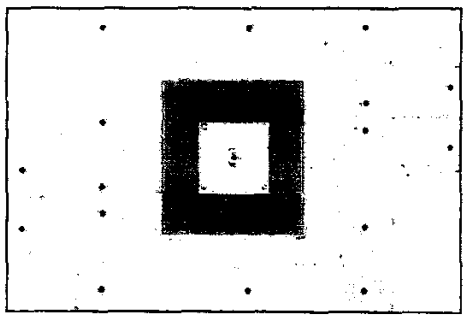

Fig. 3 *Experimental prototype (top view)*

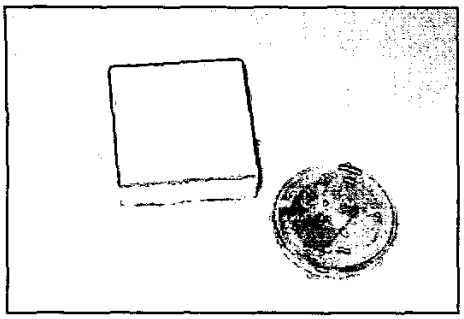

Fig. 4 *Shielded resonator*

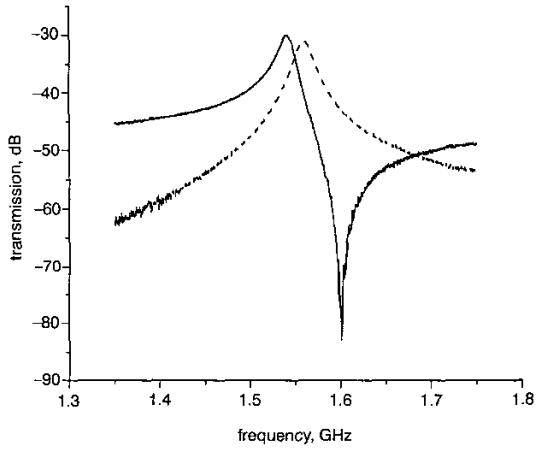

Fig. 5 *Measurements of transmission coefficient*
——— shielded resonator
..... unshielded resonator

Experimental results: A prototype of the resonator has been fabricated and tested. Fig. 3 shows the unshielded resonator. Two microstrip lines are weakly coupled by proximity to the resonator enabling a transmission-type measurement of both the resonant frequency and quality factor [4]. A first metallised layer is printed on a 635 μm thick Al_2O_3 substrate having $\varepsilon_r = 9.8$. The metallic ring and the microstrip lines are realised on this layer. A second ceramic 40 μm thick layer is stacked, with an upper metallised square patch. The patch side is of 5.74 mm. Coplanar waveguide (CPW) access is used to enable top shielding of the structure. A cover has been realised in foam dielectric block machined to realise a small cavity. The inner part of the cavity has been silver plated to realise electromagnetic shielding. The plating is interrupted at two small regions to let the CPW lines enter the cavity. No interference is observed between the CPW access and the cover at this point because of the electrical transparency of the foam material ($\varepsilon_r = 1.07$, tg $\delta = 10^{-3}$). The cover is then placed on top of the resonator and a view of the assembled resonator is shown in Fig. 4. The measured resonant frequency is of 1.54 GHz while the unloaded quality factor is of 122. Fig. 5 shows the transmission coefficient of the shielded and unshielded resonator in the frequency band 1.35–1.75 GHz. The main effect of the cover is to slightly down shift the resonant frequency (~20 MHz) and to increase the unloaded quality factor (from 80 to 122). A transmission zero, that is not observed in the case of the unshielded resonator, appears, which corresponds to the additional coupling effects induced by the packaging between the input/ouput feeding access.

Conclusion: A novel miniature multilayer resonator suitable for band-pass multilayer ceramic filters has been presented in this Letter. The structure is an evolution of the wired-patch resonator previously introduced by the authors. The actual structure strongly decreases the resonant frequency of the parallel mode (a simple layer rectangular wired-patch resonator having the same dimensions and printed on the same substrate resonates at 4.16 GHz while the actual resonant frequency is 1.54 GHz) enabling an important reduction of the patch surface for a given frequency. A simple layer squared patch of side 31 mm, printed on the same substrate, resonates at the same frequency of 1.54 GHz on its parallel mode, the actual side of the multilayer patch is of 5.74 mm.

Experimental results show interesting values of the resonator quality factor that set it as suitable for passive filter applications.

13 June 2002
Electronics Letters Online No: 20020772
DOI: 10.1049/el:20020772

M. Simeoni and S. Verdeyme (*Institute of Research for Optical and Microwave Communications (IRCOM), CNRS/University of Limoges, France*)

E-mail: msimeoni@ieee.org

C. Person (*Ecole Nationale Supérieure des Télécommunications (ENST), Brest, France*)

References

1 SIMEONI, M., VERDEYME, S., BAILLARGEAT, D., and GUILLON, P.: 'Résonateur Planaire Passif Compact pour des Applications au Filtrage Microondes'. Proceeding of the Conference 12èmes Journées Nationales Microondes, Poitiers, France, May 2001
2 YAN, Z.: 'A Microstrip patch resonator with a via connecting ground plane', *Microw. Opt. Technol. Lett.*, 2002, **32**, (1), pp. 9–11(Wiley)
3 DELAVEAUD, CH., LEVEQUE, PH., and JECKO, B.: 'New kind of microstrip antenna: the monopolar wire-patch antenna', *Electron. Lett.*, 1994, **30**, (1)
4 KAJFEZ, D.: 'Q Factor', *Vector Forum, Oxford MS*, 1994

Robot trajectory control using neural networks

Ş. Yildirim

The use of a new type of neural network (NN) for controlling the trajectory of a robot is discussed. A control system is described which comprises an NN-based controller and a fixed-gain feedback controller. The NN-based controller employs a modified recurrent NN, the weights of which are obtained by training another NN to identify on-line the inverse dynamics of the robot. The work has confirmed the superiority of the proposed NN-based control system in rejecting large disturbances.

Introduction: Robot manipulators have become increasingly important in the field of flexible automation in recent years. Programmability, high speed and high precision are some of the qualities they possess which are desirable for flexible automation. However, recently, neural network (NN)-based control approaches have been developed that do not require prior knowledge about the plant to be controlled. For example, [1, 2] have presented control architectures using NNs that are efficient at learning nonlinear motion control tasks from input and output data obtained from the plant. Yildirim and Uzmay [3] have described the training of NNs to model the forward and inverse dynamics of plants and have applied the trained NNs to the control of a robot arm. The proposed control scheme is able to adapt to changes in the operating conditions and dynamics' parameters of the arm.